Journal of Applied Physics

Fabrication of interdigitated electrodes of graphene oxide/silica by femtosecond laser-induced forward transfer for sensing applications

Cite as: J. Appl. Phys. **133**, 053103 (2023); https://doi.org/10.1063/5.0137926
Submitted: 06 December 2022 • Accepted: 17 January 2023 • Published Online: 06 February 2023

Kelly T. Paula, Sabrina N. C. Santos, Murilo H. M. Facure, et al.

Journal of Applied Physics ARTICLE scitation.org/journal/jap

Fabrication of interdigitated electrodes of graphene oxide/silica by femtosecond laser-induced forward transfer for sensing applications

Cite as: J. Appl. Phys. **133**, 053103 (2023); doi: 10.1063/5.0137926
Submitted: 6 December 2022 · Accepted: 17 January 2023 ·
Published Online: 6 February 2023 · Corrected: 8 February 2023

Kelly T. Paula,[1] Sabrina N. C. Santos,[1] Murilo H. M. Facure,[2,3] Francineide L. Araujo,[1] Marcelo B. Andrade,[1] Daniel S. Correa,[2,3] and Cleber R. Mendonça[1,a)]

AFFILIATIONS

[1]São Carlos Institute of Physics, University of São Paulo, 13560-970 São Carlos, SP, Brazil
[2]Nanotechnology National Laboratory for Agriculture (LNNA), Embrapa Instrumentação, 13560-970 Sao Carlos, SP, Brazil
[3]PPGQ, Department of Chemistry, Center for Exact Sciences and Technology, Federal University of Sao Carlos (UFSCar), 13565-905 Sao Carlos, SP, Brazil

[a)]**Author to whom correspondence should be addressed:** crmendon@ifsc.usp.br

ABSTRACT

Graphene-based materials, such as graphene oxide (GO), have been receiving much attention due to their graphene-like properties and compatibility with other materials. At the same time, novel printing methods have been developed for fabricating high-resolution patterns, such as Laser-Induced Forward Transfer (LIFT), which allows microscale transferring of a variety of materials to distinct substrates, enabling the design of micro- and nanodevices for biomedical and opto-electronic application. In this work, we propose the use of LIFT with fs-laser pulses for creating high-resolution interdigitated electrodes of tetraethyl orthosilicate functionalized with GO. The fs-LIFT approach successfully allowed micro-patterning of lines with widths on the order of 2 μm, with threshold energy of 70 nJ, and the reduction of graphene oxide to fabricate silica/GO films in an efficient, controlled, and localized way, without material degradation. As a proof of principle, interdigitated electrodes fabricated by fs-LIFT were successfully used as the sensing units of an impedimetric electronic tongue for taste recognition and heavy metals ions detection (Al^{3+}, Hg^{2+}, Co^{2+}, and Cu^{2+}) at different concentrations of 100 nmol l^{-1}, 10 μmol l^{-1}, and 1 mmol l^{-1}.

I. INTRODUCTION

In recent years, the fabrication of micro- and nano-components to develop high-performance devices for diverse applications has been receiving considerable attention. Novel high-resolution printing methods, along with the need to implement low-cost microarrays with high precision and reproducibility, have been widely studied.[1–4] As an alternative to standard lithographic processes, recent advances in laser processing have made possible the utilization of versatile and flexible direct laser writing (DLW) techniques, allowing excellent deposition control for various applications, such as microelectromechanical devices,[5] optical components,[6,7] sensors,[8–10] and medical systems.[11–13] In particular, Laser-Induced Forward Transfer (LIFT) is a single-step and non-destructive printing process capable of performing micropatterning and localized deposition of small amounts of a variety of solid materials, such as metals,[14–17] polymers,[18,19] semiconductors,[20] 2D materials,[21,22] metallic pastes,[23,24] biomaterials,[25,26] and even DNA solid films.[27] The LIFT process consists of irradiating, with a pulsed laser, a thin layer of a donor material, to transfer it to different types of substrates. This irradiation increases the local pressure, ejecting small pixels or droplets from the donor material onto a receiver substrate, placed close or in contact with the donor sample. To increase the spatial resolution and, at the same time, allow the deposition of intact material, LIFT has been performed with femtosecond laser pulses (fs-LIFT), which reduces thermal effects and collateral damage.

In the context of patterning sensitive materials without damaging their structure, which requires more complex deposition techniques, graphene-based materials, such as graphene oxide (GO) and reduced graphene oxide (rGO), are excellent candidates given their prospects for microelectronics applications. Because of

some similarities to graphene (such as a high specific surface area, mechanical,[28] and thermal[29,30] properties), compatibility with other materials, and its low-cost production, GO is conquering space in graphene-based electronics.

Due to oxygen-containing functional groups in its structure, GO is an electrically insulating material that requires a chemical reduction process to gain the electrical conductivity desired for electronic applications. However, the presence of these groups in GO allows the dispersion of the platelets in water as well as in other solvents, enabling their use in, for example, hydrolysis and condensation reactions.[31] Thus, GO becomes suitable and interesting for producing silica-based hybrid materials by the solgel process, which enables chemical homogeneity, high purity, low cost and ease of processing in a single step, and the possibility of production at low temperature. For the GO reduction in the silica matrix, the laser-induced reduction can be achieved upon the LIFT process, which not only removes the oxygen groups but also facilitates the printing and structuring of the material.[32,33] Hence, the combination of solgel and laser processing becomes a promising approach for fabricating structures based on silica and GO for application in microelectronics.

In this work, we employed fs-LIFT to fabricate graphene oxide/silica hybrid microstructures with widths of the order of 2 μm on glass substrates. Scanning electron microscopy (SEM) and atomic force microscopy (AFM) images revealed a controllable deposition of the material onto the target substrate. UV-vis and Raman spectroscopies revealed GO reduction upon fs-LIFT, which was corroborated by the electrical conductivity data. The process was used to fabricate interdigitated electrodes (IDEs), which were used as sensing units of an impedimetric electronic tongue (e-tongue), revealing good sensitivity towards the studied analytes.

II. EXPERIMENTAL

GO/silica solution was prepared by mixing tetraethylorthosilicate (TEOS) (purity of at least 98%, obtained from Sigma Aldrich), de-ionized water, and absolute ethanol (EtOH) in the presence of hydrochloric acid (HCl) as a catalyst and graphene oxide (powder, 4–10% edge-oxidized, obtained from Sigma Aldrich). Volumes of TEOS, EtOH, and de-ionized water were mixed and stirred for 10 min at room temperature. Afterward, 0.1 mol/L HCl was gradually added to the solution while stirring, to prepare the solgel solution with TEOS:H_2O:HCl:EtOH molar ratio of 1:4:0,1:1. Ethanol dispersion of GO with a concentration of 3 mg/ml was sonicated for 30 min to minimize cluster formation and then added in the silica solution. The hydrolysis was promoted by submitting the final solution under a constant power of ultrasonic radiation for 10 min and then stirring for 30 min for complete homogenization. The thin films were prepared from the solution described. Each sample (donor film) was spin-coated onto transparent glass substrates using 100 μl of the solution applying 4000 rpm for 10 s and dried for 2 h at N_2 atmosphere. During film deposition, the evaporation of the solvent produces a rigid solid layer. This approach resulted in GO/silica films of approximately 1.4 μm of thickness. The glass substrates underwent a simple cleaning using an ultrasonic bath in a 2M sodium hydroxide (NaOH) solution for 20 min, followed by an ultrasonic bath with de-ionized water for 10 min and then rinsing and drying at 80 °C.

To carry out the fs-LIFT experiments, we used a femtosecond laser system (diode pumped Yb:KGW) delivering 216-fs pulses at a central wavelength of 1030 nm, and 1 MHz of repetition rate was used for the transfer. A schematic displaying the basic components of a LIFT system is shown in Fig. 1. The laser beam was focused by a 0.65 of numerical aperture microscope objective (40×) at the interface between the GO/silica film and the transparent substrate. The donor GO/silica film and the glass receiver substrate were placed in contact, positioned in the *x-y-z* plane using three translation stages, allowing moving the sample with constant scan speed in the plane perpendicular to the laser propagation. The fs-LIFT process was monitored in real-time with the aid of a CCD camera and a backlight illumination. A half-wave plate and a polarizer were used to vary the pulse energy. The experiment was carried out in ambient air, under atmospheric pressure and room temperature.

The produced GO/silica microstructures were characterized by optical microscopy using a Zeiss LSM-700 microscope, scanning electron microscopy (SEM) using a FEI Inspect-F50 microscope, and also by atomic force microscopy (AFM) using a Nanosurf's easyScan 2® microscope. Optical properties were analyzed by UV-Vis spectroscopy using a Shimadzu UV-1800 spectrophotometer. Raman spectra of the donor GO/silica film, as well as the micropatterns transferred on the receptor substrate, were carried out using a LabRAM HR Evolution confocal micro-Raman system.

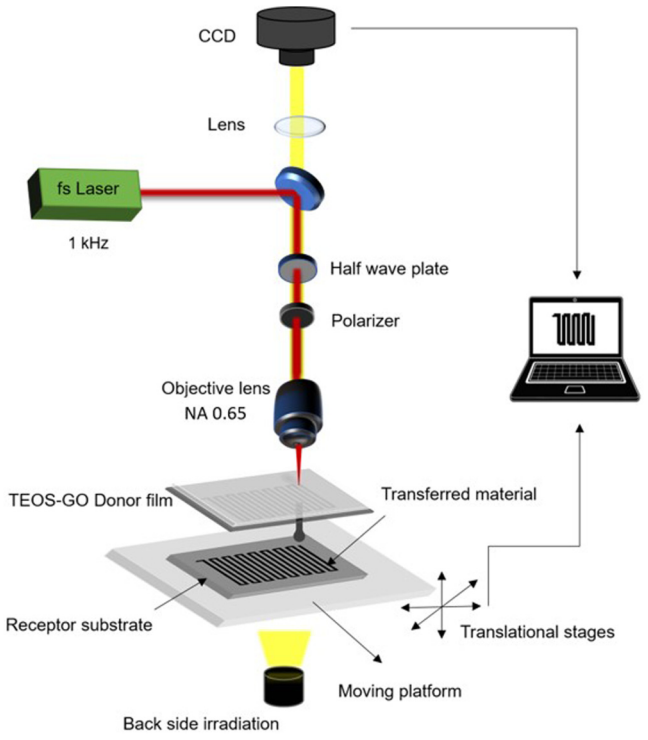

FIG. 1. Representation of the femtosecond LIFT setup.

The electrical measurements were performed with a Keithley 6487 Picoammeter and a Solartron 1260A impedance analyzer coupled to a 1296 dielectric interface. The impedance data collected by the e-tongue were treated by the principal component analysis (PCA) technique using the PEx-Sensor software.[34,35] The PCA is a technique that reduces the dimensionality of the data while retaining most of their variation. The PCA plot obtained allows the visualization of the treatment, in which the proximity of the points in the graph indicates similarities between them.[36]

III. RESULTS AND DISCUSSION

LIFT was accomplished using a 0.65 NA microscope objective for beam focusing, 50 and 100 μm/s of scanning speed, and different pulse energies. Groups of lines of 600 μm long, separated by 20 μm, were produced by LIFT to evaluate the influence of pulse energy on the line width. Figure 2(a) presents optical images of transferred lines using energies ranging from 80 to 100 nJ. From the optical microscopy images, for each group of lines, it was possible to measure the average radius (r), which increases with the energy, ranging from ~0.8 to 1.1 μm as indicated in Fig. 2(b), which presents the square of the line radius as a function of pulse energy for 50 μm/s (black circles) and 100 μm/s (gray circles). As the laser beam used for material transfer presents a Gaussian spatial distribution, from these results, it was possible to determine the threshold energy for deposition, applying the zero damage method.[37] We determined, by fitting (solid line) the experimental data presented in Fig. 2(b), threshold energies of (60 ± 10) and (70 ± 10) nJ, respectively, for scanning speeds of 50 and 100 μm/s. From the line-fittings, it was also possible to estimate the Gaussian beam radius (w_0) of 2.3 μm for both scan speeds, leading to a threshold laser fluence (F_{th}) of (0.72 ± 0.07) J/cm^2 for 50 μm/s and (0.83 ± 0.08) J/cm^2 for 100 μm/s of scanning speed. In this regime of high frequencies and low scanning speeds, we have a pulse overlapping of 99.99%, in which a large number of pulses (N ~ 60 000) hit the same area, causing a uniform distribution of intensity of the

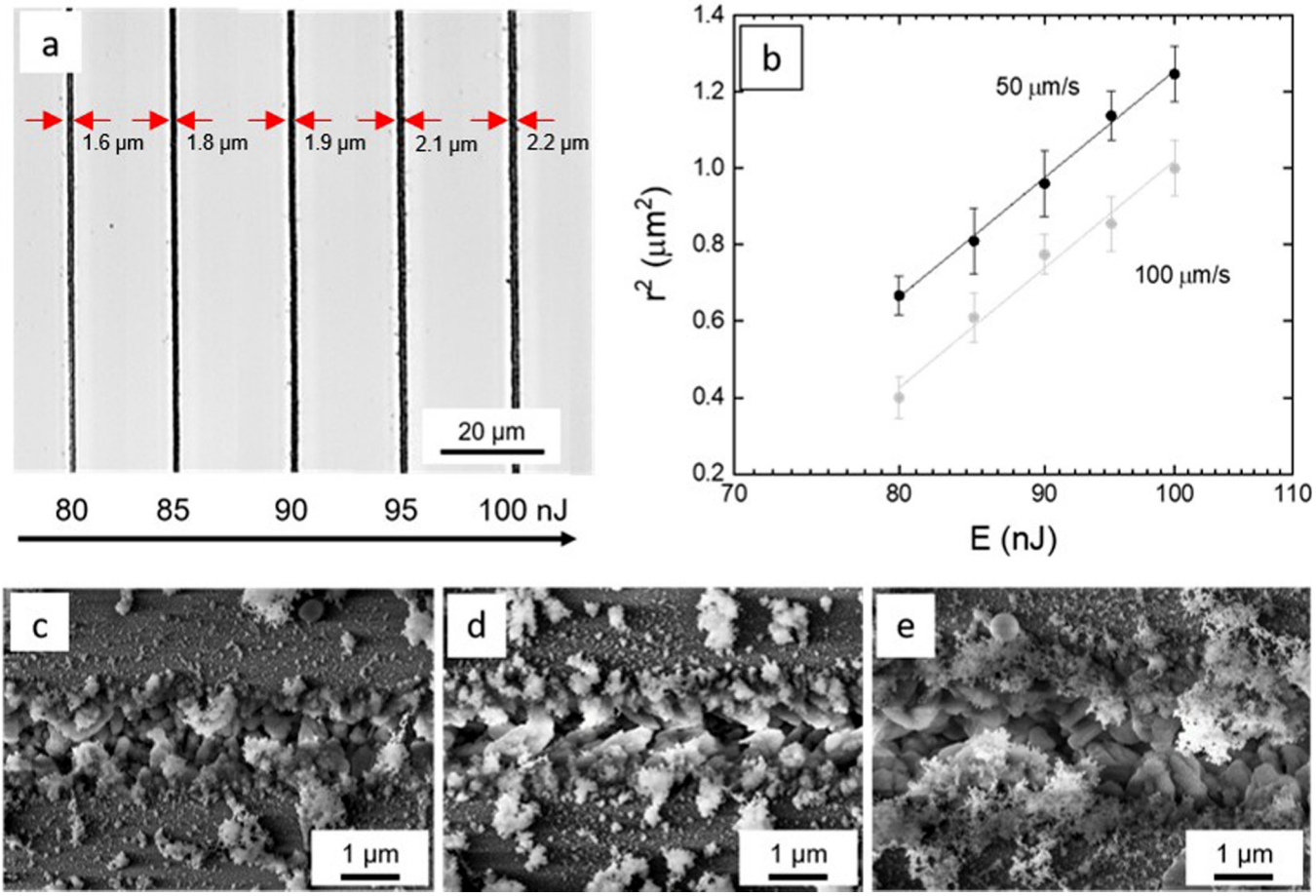

FIG. 2. (a) Optical images of fs-LIFT GO/Silica microstructures (black regions) showing the evolution of the line width with the pulse energy. (b) Line width squares as a function of the pulse energy using scanning speeds of 50 μm/s (black circles) and 100 μm/s (gray circles). The solid line is a fitting to the experimental parameters. (c)–(e) Scanning electron microscopy images of fs-LIFT GO/Silica microstructures using pulse energies of (c) 80, (d) 90, and (e) 100 nJ.

Gaussian laser beam in the center of the spot. Thus, the material removal by LIFT follows the Gaussian beam profile, as seen by the linear behavior on the squared line width as a function of the pulse energy on a linear-log scale, respectively.

To determine the optimum irradiation parameters that generate high-quality patterns, we present the SEM images of the transferred lines using 50 μm/s and different pulse energies; 80 nJ [Fig. 2(c)], 90 nJ [Fig. 2(d)], and 100 nJ [Fig. 2(e)]. For lower pulse energies, we found a homogeneous particle distribution about a central line, as observed in Figs. 2(c) and 2(d). For higher pulse energies, we have observed a non-uniform distribution with a depressed region in the central line surrounded by resolidified transferred material, as shown in Fig. 2(e). Relating to the quality of deposition, when compared to our previous work,[38] in which LIFT was used to transfer pure Graphene Oxide (GO) to a glass substrate, less energy is required and better quality is achieved when GO is transferred together with a host material.

Figure 3(a) shows an AFM image of transferred lines on the receptor substrate by fs-LIFT using a pulse energy of 90 nJ and a scanning speed of 50 μm/s. Figure 3(b) displays the AFM 3D-micrograph profile and the respective profile is shown in Fig. 3(c), from which it is possible to determine the height of the line of approximately 400 nm. From AFM results obtained for lines produced at different pulse energies, one observes, for low pulse energies (from 80 to 90 nJ), homogeneous particle distribution about a central line, with height ranging from ~200 to 400 nm, which increases when energy increases. For higher pulse energies ($\geq$95 nJ), we have observed a non-uniform distribution with a depressed region in the central line, surrounded by resolidified transferred material, being possible to determine the height of the line of about 350 nm, decreasing to higher energies (results not shown).

To investigate the optical properties, a 1×1 mm^2 area was transferred on the transparent substrate using a pulse energy of 90 nJ, a scanning speed of 50 μm/s, and 1 μm of separation between them, as shown by the SEM image in the inset of Fig. 4. Figure 4 presents the UV-vis spectra of the donor GO/Silica, represented by the black line, as well as the transferred GO/Silica on the receptor substrate by fs-LIFT, represented by the gray line. Due to the small signals involved, and the absorbance range, there is a need to proceed with background subtraction and signal optimization. The absorbance measurements of both samples were performed by the appropriate baseline correction, subtracting the measured light intensity of the reference channel, which we use the uncoated glass substrate, from the sample channel. The spectra of donor GO/Silica exhibits an absorption peak at 227 nm attributed to the π–π^* transitions of the sp^2 C=C bonds characteristic of the graphene structure.[39] Upon fs-LIFT, the absorption band is red-shifted to 260 nm, increasing the π-conjugation, requiring less energy for the transition.[39] In other words, the fs-LIFT process removes some oxygen

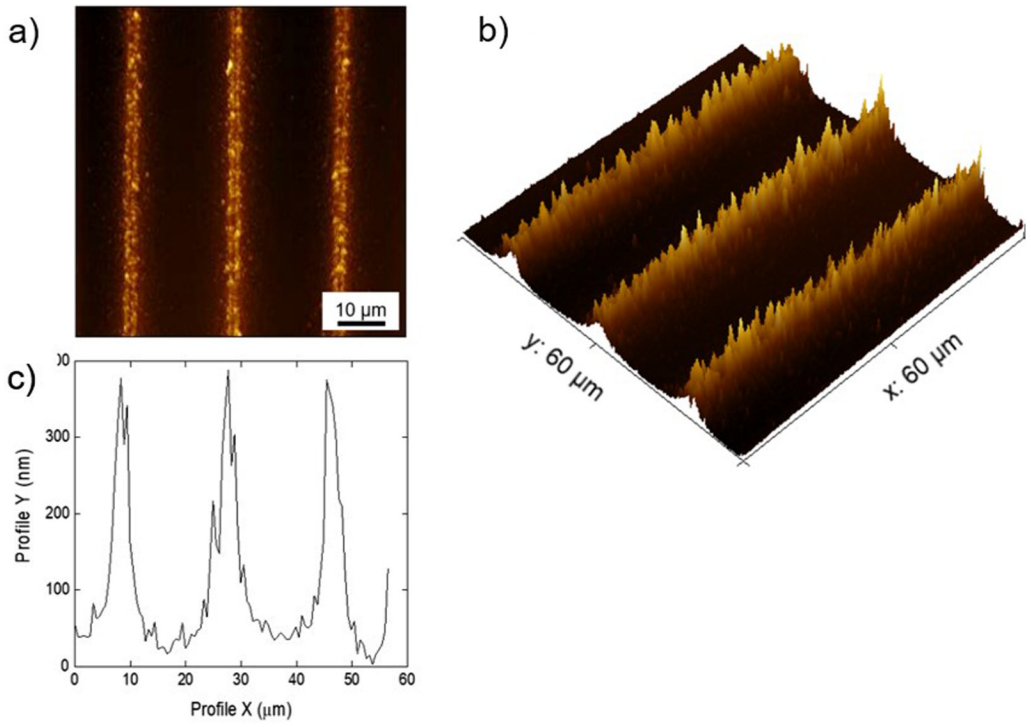

FIG. 3. (a) AFM image of transferred lines on the receptor substrate by fs-LIFT using pulse energy of 90 nJ and scanning speed of 50 μm/s, (b) the respective AFM 3D-micrograph, and(c) the respective profile trace.

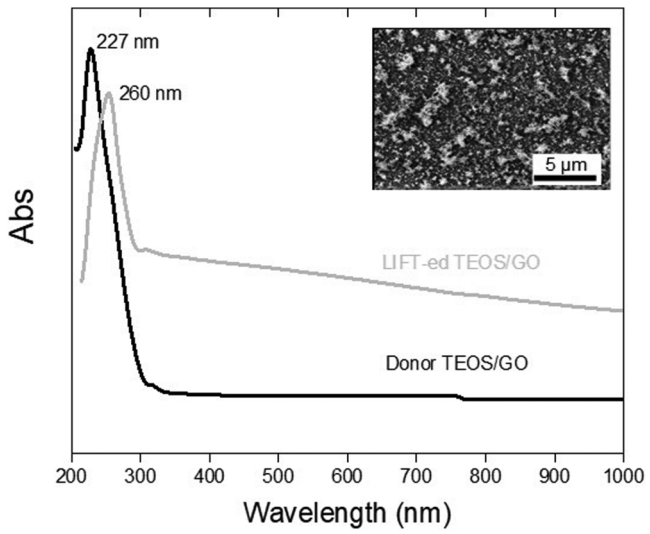

FIG. 4. UV/Vis absorption spectra of the donor GO/Silica (black line) and the transferred GO/silica on the receptor substrate by fs-LIFT (gray line). The inset shows a SEM micrograph of the transferred GO/silica on the transparent substrate using pulse energy of 90 nJ, scanning speed of 50 μm/s and 1 μm of separation between them.

functional groups of the GO structure and, in consequence, increases the amount of aromatic rings and the π-conjugation system, making it possible to excite electrons with less energy. The continuously decrease observed is characteristic of reduced graphene oxide due to the effect of increasing conjugation.[40–42]

To investigate the structural quality of the donor and transferred GO/Silica, micro-Raman spectroscopy was employed. In Fig. 5, it is possible to observe that the Raman spectrum of the fs-LIFTed GO/silica (gray line) is similar to the one of the donor material (black line). The donor GO/silica spectrum exhibits the characteristic peaks of a silica network in the region between 400 and 3500 cm^{-1}. The band at 450 cm^{-1} corresponds to the presence of methyl groups bonded to silicon (ring breathing vibration).[43,44] The Raman bands at 800, 950, and 1096 cm^{-1} correspond to symmetric vibration stretching of Si–O–Si, symmetric vibration stretching of Si-OH, and anti-symmetric vibration stretching of Si–O–C, respectively.[43–46] At 1412 and 2970 cm^{-1}, the bands observed are assigned to the CH_3 anti-symmetric bending and the anti-symmetric vibration stretching of CH_3, respectively.[43,47]

As shown in Fig. 5, the donor GO/silica Raman spectrum exhibits the G peak at 1581 cm^{-1}, corresponding to the first-order scattering of the E_{2g} mode,[48] while the D band at 1340 cm^{-1} is a breathing mode of κ-point phonons of A_{1g} symmetry. From such data, the intensities ratio (I_D/I_G) of the D and G bands of GO was determined as 0.95.

The spectrum of the LIFTed samples also displays the characteristic peaks of TEOS and GO. In this case, it was found an I_D/I_G of 1.29. In addition, there is a G-band shift in the Raman spectrum of the LIFTed samples in comparison to the donor one. The I_D/I_G is higher for the transferred material, which can be explained as a decrease in the sp^3 domains of GO, indicating the reduction process.[49–51] The shift of the G-band to higher frequencies is ascribed to the amorphization of graphite, with the presence of double bonds.[52]

Electrical measurements were performed to evaluate the quality of GO/silica donor film, as well as of the fs-LIFTed lines for application in electronic devices. For comparison, the electrical conductivity of the donor GO/Silica sample was measured using the four-point probe method, following the approach described in Ref. 53, yielding a value of 1.2×10^{-6} S cm^{-1}. For fs-LIFTed GO/silica, a 2×2 mm^2 area with lines in close proximity, separated by 2 μm, without overlapping, using 90 nJ of pulse energy and 50 μm/s of scanning speed was transferred onto Gold (Au) contacts, as schematic illustrated in Fig. 6(a). In Fig. 6(b) we present a current–voltage ($I \times V$) curve for fs-LIFTed GO/silica film of 400 nm-thickness (estimated by AFM), which displays an ohmic behavior. The electrical resistance was calculated with the respective geometric pattern, whose corresponding electrical conductivity is 1.4×10^{-3} S cm^{-1}, a value of three orders of magnitude greater than the donor GO/silica film, and of the same order of other graphene oxide-based composites and carbon materials.[54–56] This indicates an improvement in electrical conductivity after the fs-LIFT process due to the chemical reduction of GO, corroborating with the UV-visible absorption and Raman spectroscopy measurements.

By using LIFT, we fabricated interdigitated electrodes (IDEs), using the optimum irradiation parameters, determined as 90 nJ of pulse energy and 50 μm/s of scanning speed, whose geometry can be varied by controlling the movement of the *xy* stage during the laser fabrication process. The fabricated IDEs were tested for sensing applications. For that, impedance measurements were performed using three electrodes with different geometries: E1 with 40

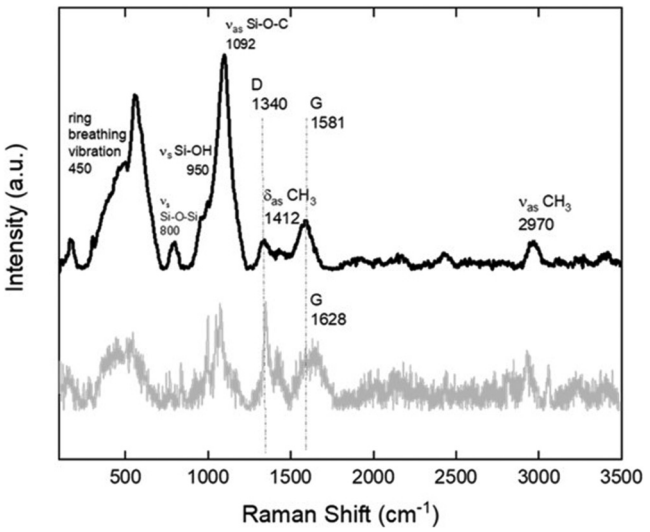

FIG. 5. Raman spectrum of donor GO/silica (black line) and LIFTed GO/silica (gray line) samples.

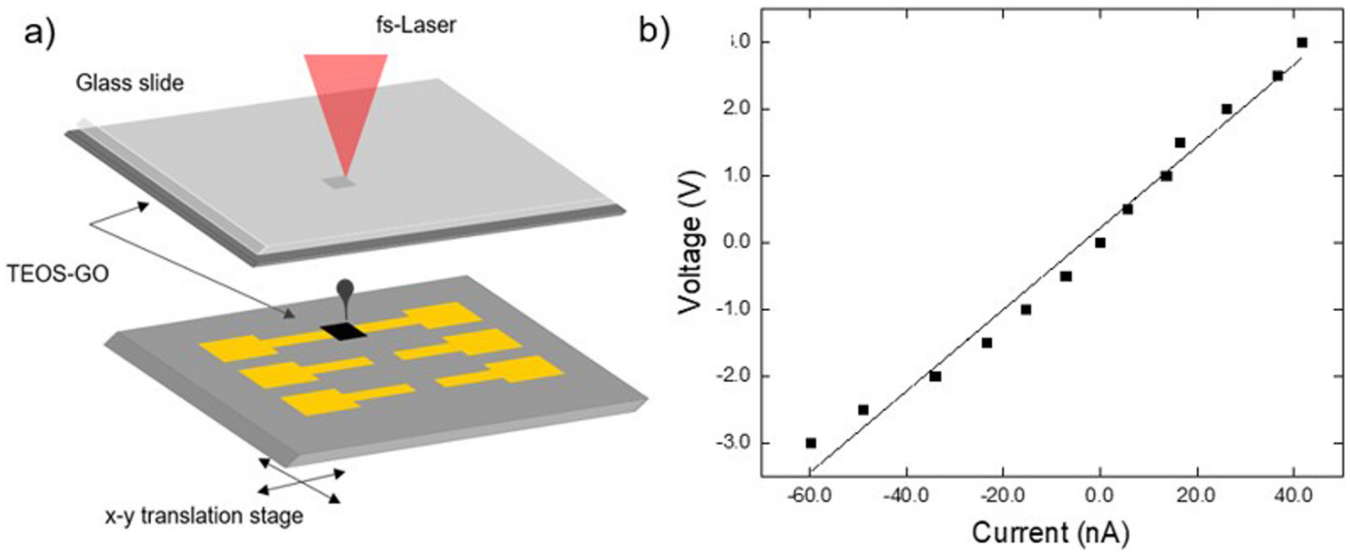

FIG. 6. (a) Illustration of the experimental setup employed to transfer by fs-LIFT GO/silica samples onto the Gold (Au) electrodes. (b) Current–voltage (I × V) curve for fs-LIFTed GO/silica.

digits spaced by 10 μm, E2 with 40 digits spaced by 20 μm, and E3 with 40 digits spaced by 30 μm, as shown in Fig. 7.

Electrical impedance spectroscopy was first used to characterize the electrodes.[57] Measurements were performed using double-distilled water (20 μl) and varying the frequency from 1 MHz to 10 Hz. The Nyquist plots obtained for the three electrodes are shown in Fig. 8(a). The data were fitted using the equivalent circuit shown in the inset of Fig. 8(a). The values of the elements in the equivalent circuit for each electrode are presented in Table I. The obtained values show that the capacitance (CPE1-T) of the electrodes

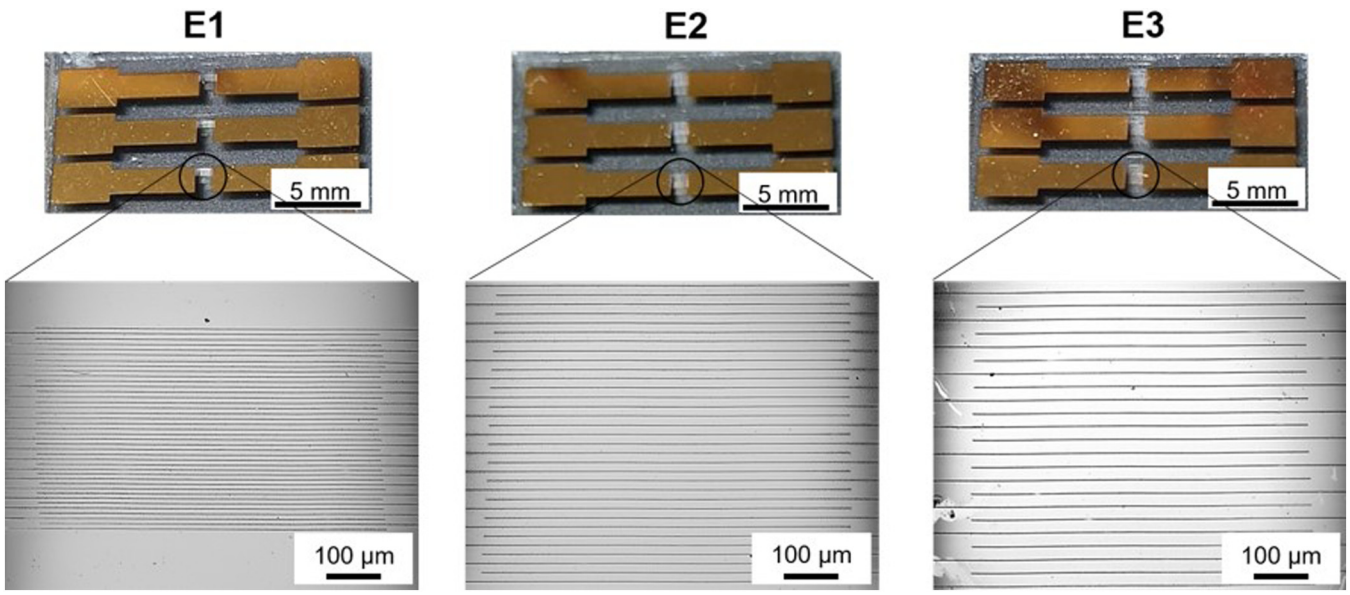

FIG. 7. Images of the fabricated electrodes: E1 (digits spaced by 10 μm), E2 (digits spaced by 20 μm), and E3 (digits spaced by 30 μm) and their respective optical micrographs.

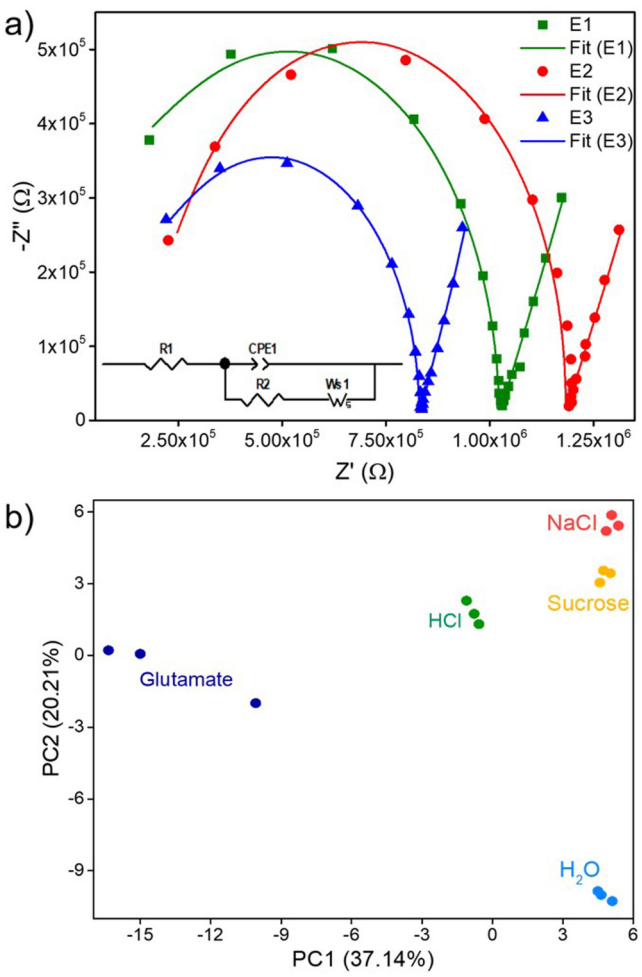

FIG. 8. (a) Nyquist plots for E1, E2, and E3 and the equivalent circuit used to fit the impedance data collected. (b) PCA plot obtained by treating the Z′ and Z″ data collected using the electrodes E1, E2, and E3 for the analyses of NaCl, sucrose, HCl, glutamate, and water.

TABLE I. Values of the elements present in the equivalent circuit obtained to fit the impedance data collected for the electrodes E1, E2, and E3.

Element	E1	E2	E3
R1 (Ω)	7381	2.00×10^5	1.18×10^5
CPE1-T (F)	1.14×10^{-12}	1.17×10^{-12}	1.48×10^{-12}
CPE1-P	1.01	1.05	1.02
R2 (Ω)	1.01×10^6	9.79×10^5	7.11×10^5
Ws1-R ($\Omega\,s^{-1/2}$)	2.08×10^6	1.89×10^6	1.73×10^6
Ws1-T ($\Omega\,s^{-1/2}$)	0.22	0.24	0.19
Ws1-P ($\Omega\,s^{-1/2}$)	0.69	0.68	0.73

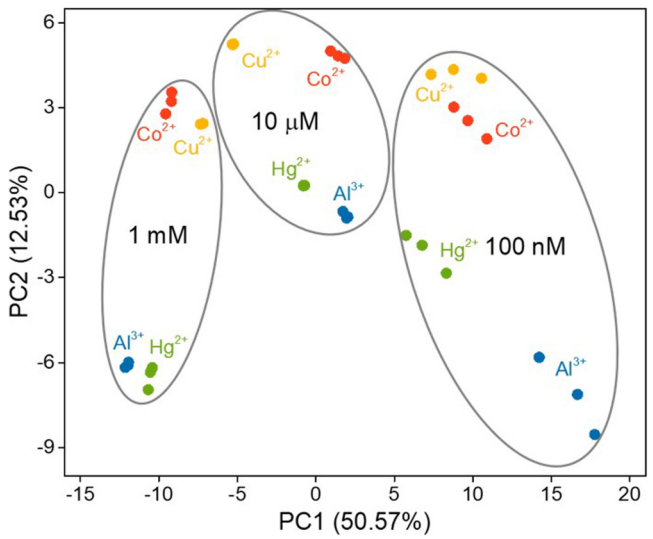

FIG. 9. PCA plot obtained by treating the data collected using the three electrodes in the impedance measurements for the analyses of the metal ions.

increased from E1 to E3, which is in accordance with the distance between the digits, i.e., smaller for E1 and larger for E3.[58,59]

Subsequently, the IDEs were used as sensing units of an e-tongue. To investigate the ability of the system in discriminating different tastes, the analyses were performed using NaCl, sucrose, HCl, and glutamate solutions to mimic salty, sweet, sour, and umami flavors, respectively. The solutions were prepared at 0.1 mmol/l and the Z′ and Z″ data collected were treated. As can be seen in Fig. 8(b), the system was able to differentiate the flavors, indicating their potential to be used as sensing units of an e-tongue.[60] It can be seen that no superposition of different samples occurred and that the triplicate points are close to each other, which indicates high reproducibility of the system.[61]

To further evaluate the discrimination capability of the e-tongue composed of three distinct electrodes, analyses of heavy metal ions (Al^{3+}, Hg^{2+}, Co^{2+}, and Cu^{2+}) were performed at different concentrations, i.e., 100 nmol l^{-1}, 10 μmol l^{-1}, and 1 mmol l^{-1}. Through the impedance data (Z′ and Z″) treatment, the system was able to differentiate the heavy metal ions and group the samples with the same concentration, as shown in Fig. 9. Again, there is no superposition between different groups and the triplicate points of the same sample are close to each other, indicating the reproducibility of the measurements. The discrimination efficiency of the e-tongue was validated by the silhouette coefficient (SC), which was found to be 0.89. An SC value closer to unity indicates greater discrimination of the samples.[62,63] The graph represents 63.1% (PC1 + PC2) of all the variance collected by the system.

The results show that the fabricated IDEs represent an easy and reliable alternative to be used as sensing units of e-tongues and other sensing devices. In addition, the IDEs can be functionalized with other sensing materials in order to attain higher sensitivity

and specific analytes interactions, which can lead to enhanced sensing performances towards specific analytes.[64–66]

IV. CONCLUSIONS

We have demonstrated the successful fabrication of graphene oxide/silica interdigitated electrodes using femtosecond laser-induced forward transfer and their application in an electronic tongue for taste and heavy metals sensing. The fs-LIFT technique, combined with the advantages of the solgel process, offers an approach for patterning graphene-based materials without intermediate steps and chemical treatments in an efficient and controlled way. The transferring of lines with widths of the order of 2 μm was achieved with a threshold energy of 70 nJ. An increase in the electrical conductivity was observed for the fs-LIFTed material, supporting the material characterization results, indicating the chemical reduction of the GO in the silica matrix upon the fs-LIFT process. The ability of controlled deposition allowed the fabrication of interdigitated electrodes with high resolution, which were successfully used as sensing units for an electronic tongue, able to detect and differentiate heavy metal ions in aqueous solutions. In principle, the proposed approach can also be extended to other sensing materials, enabling customizing sensor sensitivity and selectivity to improve sensor performance towards varied analytes.

ACKNOWLEDGMENTS

The authors are grateful to São Paulo Research Foundation (FAPESP, Grant Nos. 2018/11283-7, 2017/10582-8, and 2018/22214-6), Coordenação de Aperfeiçoamento de Pessoal de Nível Superior (CAPES)—Finance Code 001, CNPq, Army Research Laboratory (No. W911NF-17-1-0123), MCTI-SisNano (No. CNPq/402.287/2013-4), Rede Agronano (EMBRAPA), and Air Force Office of Scientific Research (No. FA9550-12-1-0028).

AUTHOR DECLARATIONS

Conflict of Interest

The authors have no conflicts to disclose.

Author Contributions

Kelly T. Paula: Conceptualization (equal); Data curation (equal); Formal analysis (equal); Investigation (equal); Methodology (equal); Writing – original draft (equal); Writing – review & editing (equal). **Sabrina N. C. Santos:** Conceptualization (equal); Data curation (equal); Formal analysis (equal); Investigation (equal); Writing – original draft (equal). **Murilo H. M. Facure:** Data curation (equal); Formal analysis (equal); Writing – original draft (equal). **Francineide L. Araujo:** Data curation (equal); Writing – review & editing (equal). **Marcelo B. Andrade:** Data curation (equal); Writing – review & editing (equal). **Daniel S. Correa:** Conceptualization (equal); Formal analysis (equal); Funding acquisition (equal); Investigation (equal); Methodology (equal); Resources (equal); Writing – review & editing (equal). **Cleber R. Mendonça:** Conceptualization (equal); Formal analysis (equal); Funding acquisition (equal); Investigation (equal); Methodology (equal); Project administration (equal); Resources (equal); Writing – review & editing (equal).

DATA AVAILABILITY

The data that support the findings of this study are available from the corresponding author upon reasonable request.

REFERENCES

[1]D. Ahn, L. M. Stevens, K. Zhou, and Z. A. Page, "Rapid high-resolution visible light 3D printing," ACS Cent. Sci. **6**, 1555–1563 (2020).
[2]D. Song, A. Mahajan, E. B. Secor, M. C. Hersam, L. F. Francis, and C. D. Frisbie, "High-resolution transfer printing of graphene lines for fully printed, flexible electronics," ACS Nano **11**, 7431–7439 (2017).
[3]J.-U. Park, M. Hardy, S. J. Kang, K. Barton, K. Adair, D. K. Mukhopadhyay *et al.*, "High-resolution electrohydrodynamic jet printing," Nat. Mater. **6**, 782–789 (2007).
[4]G. B. Blancheta, Y. L. Loo, J. A. Rogers, F. Gao, and C. R. Fincher, "Large area, high resolution, dry printing of conducting polymers for organic electronics," Appl. Phys. Lett. **82**, 463–465 (2003).
[5]H. C. Tapalian, J. Langseth, Y. Chen, J. W. Anderegg, and J. Shinar, "Ultrafast laser direct-write actuable microstructures," Appl. Phys. Lett. **93**, 243304–243304 (2008).
[6]Z. Wang, K. Sugioka, and K. Midorikawa, "Fabrication of integrated microchip for optical sensing by femtosecond laser direct writing of Foturan glass," Appl. Phys. A **93**, 225–229 (2008).
[7]E. Zgraggen, I. M. Soganci, F. Horst, P. A. La, R. Dangel, B. J. Offrein *et al.*, "Laser direct writing of single-mode polysiloxane optical waveguides and devices," J. Light. Technol. **32**, 3036–3042 (2014).
[8]J. Cai, C. Lv, E. Aoyagi, S. Ogawa, and A. Watanabe, "Laser direct writing of a high-performance all-graphene humidity sensor working in a novel sensing mode for portable electronics," ACS Appl. Mater. Interfaces **10**, 23987–23996 (2018).
[9]W. Zhou, Y. Yu, S. Bai, and A. Hu, "Laser direct writing of waterproof sensors inside flexible substrates for wearable electronics," Opt. Laser Technol. **135**, 106694 (2021).
[10]A. Piqué, D. B. Chrisey, R. C. Y. Auyeung, J. Fitz-Gerald, H. D. Wu, R. A. McGill *et al.*, "A novel laser transfer process for direct writing of electronic and sensor materials," Appl. Phys. A: Mater. Sci. Process. **69**, S279–84 (1999).
[11]T. H. Au, D. T. Trinh, Q. C. Tong, D. B. Do, D. P. Nguyen, M. H. Phan *et al.*, "Direct laser writing of magneto-photonic sub-microstructures for prospective applications in biomedical engineering," Nanomaterials **7**, 105 (2017).
[12]N. R. Schiele, D. B. Chrisey, and D. T. Corr, "Gelatin-based laser direct-write technique for the precise spatial patterning of cells," Tissue Eng. Part C: Methods **17**, 289–298 (2011).
[13]S. D. Gittard and R. J. Narayan, "Laser direct writing of micro- and nano-scale medical devices," Expert Rev. Med. Devices **7**, 343–356 (2010).
[14]C. W. Visser, R. Pohl, C. Sun, G.-W. Römer, B. Huis In 'T Veld, and D. Lohse, "Toward 3D printing of pure metals by laser-induced forward transfer," Adv. Mater. **27**, 4087–4092 (2015).
[15]H. Yamada, T. Sano, T. Nakayama, and I. Miyamoto, "Optimization of laser-induced forward transfer process of metal thin films," Appl. Surf. Sci. **197–198**, 411–415 (2002).
[16]R. Molina, M. Ertuğrul, N. R. Larrea, V. Rico, F. Yubero *et al.*, "Laser-induced scanning transfer deposition of silver electrodes on glass surfaces: A green and scalable technology," Appl. Surf. Sci. **556**, 149673 (2021).
[17]C. K. P. Vallabh, Y. Xiong, and X. Zhao, "3D printing of liquid metal EGaIn through laser induced forward transfer: A proof-of-concept study," Manuf. Lett. **28**, 42–45 (2021).
[18]J. Shaw-Stewart, T. Lippert, M. Nagel, F. Nüesch, and A. Wokaun, "Laser-induced forward transfer of polymer light-emitting diode pixels with increased charge injection," ACS Appl. Mater. Interfaces **3**, 309–316 (2011).

[19]J. M. P. Almeida, O. I. Avila, M. B. Andrade, J. C. Stefanelo, A. J. G. Otuka, K. T. Paula *et al.*, "Micropatterning of poly(p-phenylene vinylene) by femtosecond laser induced forward transfer," Polym. Int. **68**, 160–163 (2019).
[20]L. Rapp, C. Cibert, S. Nénon, A. P. Alloncle, M. Nagel, T. Lippert *et al.*, "Improvement in semiconductor laser printing using a sacrificial protecting layer for organic thin-film transistors fabrication," Appl. Surf. Sci. **257**, 5245–5249 (2011).
[21]G. Li, X. Mo, W.-C. Law, and K. C. Chan, "3D printed graphene/nickel electrodes for high areal capacitance electrochemical storage," J. Mater. Chem. A **7**, 4055–4062 (2019).
[22]N. T. Goodfriend, S. Y. Heng, O. A. Nerushev, A. V. Gromov, A. V. Bulgakov, M. Okada *et al.*, "Blister-based-laser-induced-forward-transfer: A non-contact, dry laser-based transfer method for nanomaterials," Nanotechnology **29**, 385301 (2018).
[23]J. Wang, R. C. Y. Auyeung, H. Kim, N. A. Charipar, and A. Piqué, "Three-dimensional printing of interconnects by laser direct-write of silver nanopastes," Adv. Mater. **22**, 4462–4466 (2010).
[24]E. Turkoz, M. Morales, S. Y. Kang, A. Perazzo, H. A. Stone, C. Molpeceres *et al.*, "Laser-induced forward transfer from healing silver paste films," Appl. Phys. Lett. **113**, 221601–221605 (2018).
[25]J. M. Fernández-Pradas, M. Colina, P. Serra, J. Domínguez, and J. L. Morenza, "Laser-induced forward transfer of biomolecules," Thin Solid Films **453–454**, 27–30 (2004).
[26]A. Karaiskou, I. Zergioti, C. Fotakis, M. Kapsetaki, and D. Kafetzopoulos, "Microfabrication of biomaterials by the sub-ps laser-induced forward transfer process," Appl. Surf. Sci. **208–209**, 245–249 (2003).
[27]M. Colina, P. Serra, J. M. Fernández-Pradas, L. Sevilla, and J. L. Morenza, "DNA deposition through laser induced forward transfer," Biosens. Bioelectron. **20**, 1638–1642 (2005).
[28]C. Lee, X. Wei, J. W. Kysar, and J. Hone, "Measurement of the elastic properties and intrinsic strength of monolayer graphene," Science **321**, 385–388 (2008).
[29]D. Teweldebrhan, C. N. Lau, S. Ghosh, A. A. Balandin, W. Bao, I. Calizo *et al.*, "Superior thermal conductivity of single-layer graphene," Nano Lett. **8**, 902–907 (2008).
[30]A. A. Balandin, "Thermal properties of graphene and nanostructured carbon materials," Nat. Mater. **10**, 569–581 (2011).
[31]C. Hintze, K. Morita, R. Riedel, E. Ionescu, and G. Mera, "Facile sol-gel synthesis of reduced graphene oxide/silica nanocomposites," J. Eur. Ceram. Soc. **36**, 2923–2930 (2016).
[32]Y. Zhang, L. Guo, S. Wei, Y. He, H. Xia, Q. Chen *et al.*, "Direct imprinting of microcircuits on graphene oxides film by femtosecond laser reduction," Nano Today **5**, 15–20 (2010).
[33]S. Evlashin, P. Dyakonov, R. Khmelnitsky, S. Dagesyan, A. Klokov, A. Sharkov *et al.*, "Controllable laser reduction of graphene oxide films for photoelectronic applications," ACS Appl. Mater. Interfaces **8**, 28880–28887 (2016).
[34]F. V. Paulovich, M. C. F. Oliveira, and R. Minghim, "The projection explorer: A flexible tool for projection-based multidimensional visualization," in *Proceedings of the SIBGRAPI 2007—20th Brazilian Symposium on Computer Graphics and Image Processing* (IEEE, 2007), pp. 27–34.
[35]F. V. Paulovich, M. L. Moraes, R. M. Maki, M. Ferreira, O. N. Oliveira, and M. C. F. De Oliveira, "Information visualization techniques for sensing and biosensing," Analyst **136**, 1344–1350 (2011).
[36]F. E. Steffens, "What is principal components analysis?," Seminar on Principal Components Analysis of Atmosphere in Earth Science Pretoria (Council for Scientific and Industrial Research Pretoria, National Program on Weather Climate Atmosphere Research CSIR-S-334, 1983), Vol. 26, pp. 3–16.
[37]J. M. Liu, "Simple technique for measurements of pulsed Gaussian-beam spot sizes," Opt. Lett. **7**, 196–198 (1982).
[38]K. T. Paula, N. B. Tomazio, O. I. A. Salas, A. J. G. Otuka, J. M. P. Almeida, M. B. Andrade *et al.*, "Femtosecond-laser selective printing of graphene oxide and PPV on polymeric microstructures," J. Mater. Sci. **56**, 11569–11577 (2021).
[39]F. T. Johra, J.-W. Lee, and W.-G. Jung, "Facile and safe graphene preparation on solution based platform," J. Ind. Eng. Chem. **20**, 2883–2887 (2014).
[40]E. Rommozzi, M. Zannotti, R. Giovannetti, C. D'amato, S. Ferraro, M. Minicucci *et al.*, "Reduced graphene oxide/TiO_2 nanocomposite: From synthesis to characterization for efficient visible light photocatalytic applications," Catalysts **8**, 598 (2018).
[41]A. H. Wazir and I. W. Kundi, "Synthesis of graphene nano sheets by the rapid reduction of electrochemically exfoliated graphene oxide induced by microwaves," J. Chem. Soc. Pakistan **38**, 11–16 (2016).
[42]T. Sharifi, D. Dorranian, and M. J. Torkamany, "Optimisation of GaAs nanocrystals synthesis by laser ablation in water," J. Exp. Nanosci. **8**, 808–817 (2013).
[43]A. Jitianu, G. Amatucci, and L. C. Klein, "Organic-inorganic sol-gel thick films for humidity barriers," J. Mater. Res. **23**, 2084–2090 (2008).
[44]A. Bertoluzza, C. Fagnano, M. Antonietta Morelli, V. Gottardi, and M. Guglielmi, "Raman and infrared spectra on silica gel evolving toward glass," J. Non-Cryst. Solids **48**, 117–128 (1982).
[45]L. De Ferri, P. P. Lottici, A. Lorenzi, A. Montenero, and E. Salvioli-Mariani, "Study of silica nanoparticles—Polysiloxane hydrophobic treatments for stone-based monument protection," J. Cult. Herit. **12**, 356–363 (2011).
[46]A. D. Chomel, P. Dempsey, J. Latournerie, D. Hourlier-Bahloul, and U. A. Jayasooriya, "Gel to glass transformation of methyltriethoxysilane: A silicon oxycarbide glass precursor investigated using vibrational spectroscopy," Chem. Mater. **17**, 4468–4473 (2005).
[47]M. C. Matos, L. M. Ilharco, and R. M. Almeida, "The evolution of TEOS to silica gel and glass by vibrational spectroscopy," J. Non-Cryst. Solids **147–148**, 232–237 (1992).
[48]D. A. Field, C. A. Ventrice, S. Park, A. Velamakanni, R. D. Piner, S. Stankovich *et al.*, "Chemical analysis of graphene oxide films after heat and chemical treatments by X-ray photoelectron and micro-Raman spectroscopy," Carbon **47**, 145–152 (2008).
[49]G. Lee, K. S. Kim, and K. Cho, "Theoretical study of the electron transport in graphene with vacancy and residual oxygen defects after high-temperature reduction," J. Phys. Chem. C **115**, 9719–9725 (2011).
[50]D. Luo, G. Zhang, J. Liu, and X. Sun, "Evaluation criteria for reduced graphene oxide," J. Phys. Chem. C **115**, 11327–11335 (2011).
[51]Z. Wei, D. Wang, S. Kim, S.-Y. Kim, Y. Hu, M. K. Yakes *et al.*, "Nanoscale tunable reduction of graphene oxide for graphene electronics," Science **328**, 1373–1376 (2010).
[52]K. N. Kudin, B. Ozbas, H. C. Schniepp, R. K. Prud'homme, I. A. Aksay, and R. Car, "Raman spectra of graphite oxide and functionalized graphene sheets," Nano Lett. **8**, 36–41 (2008).
[53]K. T. Paula, M. V. Santos, M. H. M. Facure, M. B. Andrade, F. L. Araújo, D. S. Correa *et al.*, "Laser patterning and induced reduction of graphene oxide functionalized silk fibroin," Opt. Mater. **99**, 109540 (2020).
[54]S. Stankovich, D. A. Dikin, G. H. B. Dommett, K. M. Kohlhaas, E. J. Zimney, E. A. Stach *et al.*, "Graphene-based composite materials," Nature **442**, 282–286 (2006).
[55]S. Papazoglou, Y. S. Raptis, S. Chatzandroulis, and I. Zergioti, "A study on the pulsed laser printing of liquid-phase exfoliated graphene for organic electronics," Appl. Phys. A **117**, 301–306 (2014).
[56]D. D. L. Chung, "Review: Electrical application of carbon materials," Journal Of Materials Science **9**, 2645–2661 (2004).
[57]M. H. M. Facure, M. L. Braunger, L. A. Mercante, L. G. Paterno, A. Riul, and D. S. Correa, *Electrical Impedance-Based Electronic Tongues: Principles, Sensing Materials, Fabrication Techniques and Applications* (Elsevier Inc., 2021).
[58]Y. Xu, C. Li, W. Mei, M. Guo, and Y. Yang, "Equivalent circuit models for a biomembrane impedance sensor and analysis of electrochemical impedance spectra based on support vector regression," Med. Biol. Eng. Comput. **57**, 1515–1524 (2019).
[59]M. Takahashi, Y. Noguchi, and M. Miyayama, "Estimation of ionic and hole conductivity in bismuth titanate polycrystals at high temperatures," Solid State Ionics **172**, 325–329 (2004).

[60]A. Riul, A. M. G. Soto, S. V. Mello, S. Bone, D. M. Taylor, and L. H. C. Mattoso, "An electronic tongue using polypyrrole and polyaniline," Synth. Met. **132**, 109–116 (2003).
[61]A. Riul, C. A. R. Dantas, C. M. Miyazaki, and O. N. Oliveira, "Recent advances in electronic tongues," Analyst **135**, 2481–2495 (2010).
[62]R. S. Andre, M. H. M. Facure, L. A. Mercante, and D. S. Correa, "Electronic nose based on hybrid free-standing nanofibrous mats for meat spoilage monitoring," Sens. Actuators B: Chem. **353**, 131114 (2022).
[63]P. J. Rousseeuw, "Silhouettes: A graphical aid to the interpretation and validation of cluster analysis," J. Comput. Appl. Math. **20**, 53–65 (1987).
[64]L. A. Mercante, R. S. Andre, M. H. M. Facure, L. Fugikawa-Santos, and D. S. Correa, "Design of a bioelectronic tongue for glucose monitoring using zinc oxide nanofibers and graphene derivatives," Sens. Actuators Rep. **3**, 100050 (2021).
[65]J. C. Soares, A. C. Soares, M. K. S. C. Angelim, J. L. Proença-Modena, P. M. Moraes-Vieira, L. H. C. Mattoso *et al.*, "Diagnostics of SARS-CoV-2 infection using electrical impedance spectroscopy with an immunosensor to detect the spike protein," Talanta **239**, 123076 (2021).
[66]M. H. M. Facure, R. Schneider, D. M. dos Santos, and D. S. Correa, "Impedimetric electronic tongue based on molybdenum disulfide and graphene oxide for monitoring antibiotics in liquid media," Talanta **217**, 121039 (2020).